



Trans. Nonferrous Met. Soc. China 34(2024) 3265-3281

Transactions of Nonferrous Metals Society of China

www.tnmsc.cn



Improving comprehensive properties of Cu-11.9Al-2.5Mn shape memory alloy by adding multi-layer graphene carried by Cu₅₁Zr₁₄ inoculant particles

Zhi-xian JIAO^{1,2}, Qing-zhou WANG², Yan-jun DING³, Fu-xing YIN⁴, Chao-hui XU¹, Cui-hong HAN¹, Qi-xiang FAN¹

- 1. School of Mechanical Engineering, Tianjin University of Technology and Education, Tianjin 300222, China;
 - 2. Tianjin Key Laboratory of Materials Laminating Fabrication and Interface Control Technology, School of Materials Science and Engineering, Hebei University of Technology, Tianjin 300130, China;
 - 3. School of Materials Science and Engineering, Central South University, Changsha 410083, China;
 - 4. Institute of New Materials, Guangdong Academy of Sciences, Guangzhou 510651, China

Received 24 March 2023; accepted 20 September 2023

Abstract: In order to improve the comprehensive properties of the Cu-11.9Al-2.5Mn shape memory alloy (SMA), multilayer graphene (MLG) carried by Cu₅₁Zr₁₄ inoculant particles was incorporated and dispersed into this alloy through preparing the preform of the cold-pressed MLG-Cu₅₁Zr₁₄ composite powders. In the resultant novel MLG/Cu-Al-Mn composites, MLG in fragmented or flocculent form has a good bonding with the Cu-Al-Mn matrix. MLG can prevent the coarsening of grains of the Cu-Al-Mn SMA and cause thermal mismatch dislocations near the MLG/Cu-Al-Mn interfaces. The damping and mechanical properties of the MLG/Cu-Al-Mn composites are significantly improved. When the content of MLG reaches 0.2 wt.%, the highest room temperature damping of 0.0558, tensile strength of 801.5 MPa, elongation of 10.8%, and hardness of HV 308 can be obtained. On the basis of in-depth observation of microstructures, combined with the theory of internal friction and strengthening and toughening theories of metals, the relevant mechanisms are discussed.

Key words: Cu-Al-Mn shape memory alloy; multilayer graphene (MLG); microstructure; interface; damping; mechanical properties

1 Introduction

Cu-based shape memory alloys (SMAs) have been widely used in the fields of transportation, machinery, architecture and biomedical devices owing to their high damping capacity, special shape memory property, good processability and low cost [1–4]. However, intergranular brittle fracture and unsatisfactory mechanical strength caused by coarse grains have become the main limiting factors for their further development and extensive

applications [3–6]. Meanwhile, in order to meet the needs of vibration and noise reduction, modern industries put forward increasing requirements on damping capacity [7]. Therefore, it is extremely important to find effective ways to simultaneously improve the damping and mechanical properties of Cu-based SMAs.

Many researchers have reported that the addition of alloying elements such as Ti [8], Gd [9], Zr [10], V [11], Nb [12], Ce [13] and Nd [14] can effectively refine the grains of Cu-based SMAs, and enhance their mechanical properties. For instance,

GUNIPUTI and MURIGENDRAPPA [9] found that Gd could serve as an effective grain refiner of Cu-Al-Be SMA, which helped to improve the mechanical properties significantly. When the addition of Gd was 0.08 wt.%, the grain size of Cu-Al-Be SMA could be decreased from 463.45 to 81.80 µm. As a consequence, the tensile strength of the resultant alloy was increased from 398.93 to 581.42 MPa, and the ductility was increased from 10.05% to 23.72%. ZHANG et al [14] reported that the grain size of Cu-Al-Ni SMA could be reduced from millimeter level to several hundred microns by adding Nd, and when the content of Nd reached 0.5 wt.%, the compressive fracture stress and strain were increased from 580 MPa and 10.5% to 940 MPa and 18.3%, respectively. The increase of the mechanical properties was mainly ascribed to the grain refinement of the Cu-Al-Ni SMA with Nd addition and the hindering effect of the second phase on the movement of dislocations. Compared with the elements addition method, inoculation refinement is more efficient for grain refinement due to the high lattice matching degree between inoculants and the alloys to be refined [15–17]. In our previous work [18,19], a novel inoculant Cu₅₁Zr₁₄ was added into the Cu-Al-Mn SMA, the grains of the Cu-Al-Mn SMA could be refined from 319 to 37 µm, and the tensile strength could be increased from 352.2 to 687.2 MPa due to the fine-grain strengthening mechanism. Moreover, the damping was also significantly improved due to the increased interface density resulted from the refinement of grains.

In recent years, multilayer graphene (MLG), as a potential carbon material for strengthening metal matrix composites (MMCs), has attracted more and more attention because of its ultra-high strength and elastic modulus, easy preparation and economy compared with single-layer graphene [20-22]. Considerable attempts have been made in the fields of MLG reinforced Al [21,23], Ti [22,24] and Cu [20,25] matrix composites, and great improvements in mechanical properties have been achieved. KIM et al [20] found that the combination of high-energy ball milling and high-ratio differential speed rolling could effectively incorporate and disperse MLGs into the matrix of Cu. Due to the Orowan strengthening mechanism, a yield strength of 360.5 MPa and a tensile strength of 425.5 MPa could be obtained. KIM et al [25] obtained a MLG/Cu composite with a high strength of 1.5 GPa by preparing single-atomic-layer graphene film on the surface of Cu through chemical vapor deposition (CVD). The ultra-high strength of this new MLG/Cu nano-layered composite material could be attributed to the fact that the graphene provided an efficient barrier to the movement of dislocations across the interface.

Therefore, it is reasonable to infer that MLG can be used to improve the mechanical properties of Cu-based SMAs. And it is expected that the damping can also be improved simultaneously because of the increased interface density in the resultant composites and the typical lamellar structure of MLG. However, up to now, there are few reports on the application of MLG in Cu-based SMAs. The main challenge is the large difference in density, which makes it very difficult for MLG to be evenly distributed in Cu-based SMAs [26]. In the present study, the MLG-Cu₅₁Zr₁₄ composite powders were pre-prepared by ball-milling method. Through the role of Cu₅₁Zr₁₄ inoculant particles in carrying, MLG was dispersed in the matrix of the Cu-Al-Mn SMA. The damping and mechanical properties of the resultant novel MLG/Cu-Al-Mn composites were investigated. On the basis of in-depth observation of microstructures, combined with theory of internal friction and strengthening and toughening theories of metals, the relevant mechanisms were discussed in detail.

2 Experimental

2.1 Preparation of specimens

Figure 1(a) shows the scanning electron microscopy (SEM) image of Cu₅₁Zr₁₄ particles with an average size below 200 µm obtained by crushing the as-cast Cu₅₁Zr₁₄ ingot. Figures 1(d, e) show the analysis results of energy dispersive spectrometer (EDS) and X-ray diffractometer (XRD) of the Cu₅₁Zr₁₄ inoculant. It can be seen that the Cu₅₁Zr₁₄ inoculant only consists of the Cu₅₁Zr₁₄ phase, which belongs to intermetallic inoculant. Figures 1(b, c) show the TEM images of the MLG purchased from Wuhu Jikang New Material Technology Co., Ltd., China. It should be noted that the MLG presents many wrinkles, which can enhance both toughness and damping of the Cu-Al-Mn SMA. Figure 1(f) gives the Raman spectrum of MLG. Three peaks at 1348.03, 1581.31 and 2715.70 cm⁻¹ correspond to

the D, G and 2D bands of MLG, respectively [27].

Figure 2 shows the schematic illustration of the preparation process of the MLG/Cu–Al–Mn composites. As shown in Fig. 2, the whole process mainly includes the following three steps:

(1) Step 1: Ball milling of $Cu_{51}Zr_{14}$ and MLG composite powders

The mixtures of $Cu_{51}Zr_{14}$ particles (prepared in a WK-II vacuum arc furnace by using pure Cu

(purity ≥99.9 wt.%, Tianjin Nonferrous Metals Company, China) and Zr (purity ≥99.9 wt.%, Shenyang Scientific Research Metal Materials Co., Ltd., China) as raw materials) and MLG with different mass ratios were ball-milled at a speed of 300 r/min for 5 and 10 h in a planetary ball mill machine (QXQM−2). Stainless steel balls with diameters of 5, 8 and 10 mm (their mass ratio was 3:2:1) were used, and the ball-to-material ratio was

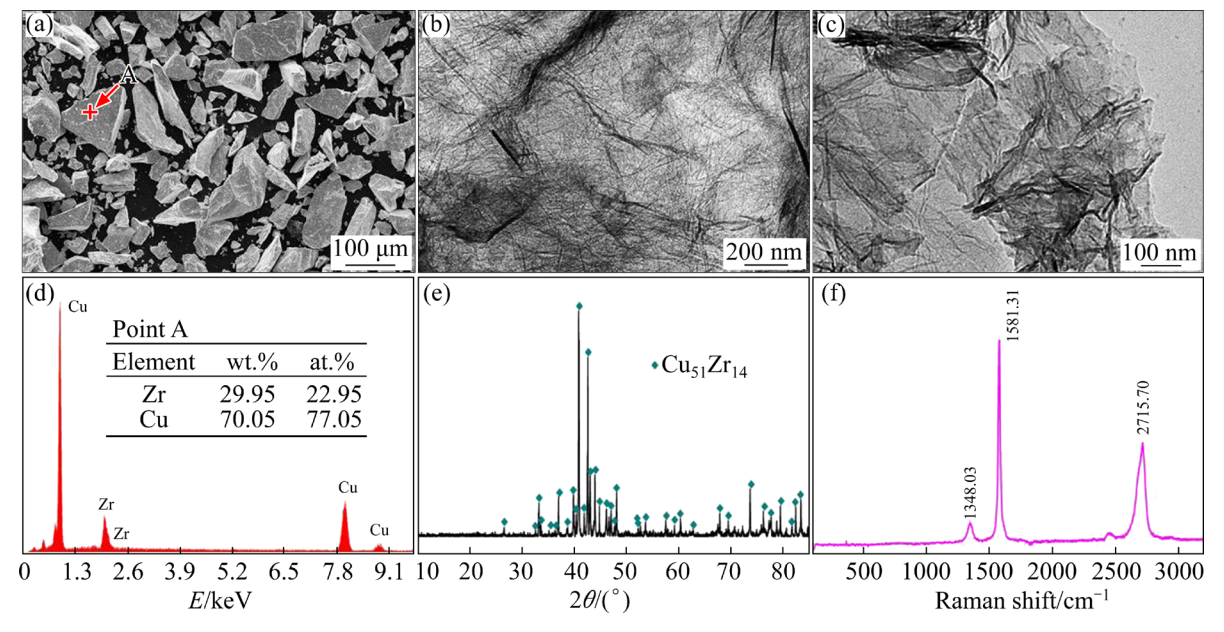


Fig. 1 SEM image of Cu₅₁Zr₁₄ inoculant (a); TEM images of MLG (b, c); EDS result (d) of Point A in (a); XRD pattern of Cu₅₁Zr₁₄ inoculant (e); Raman spectrum of MLG (f)

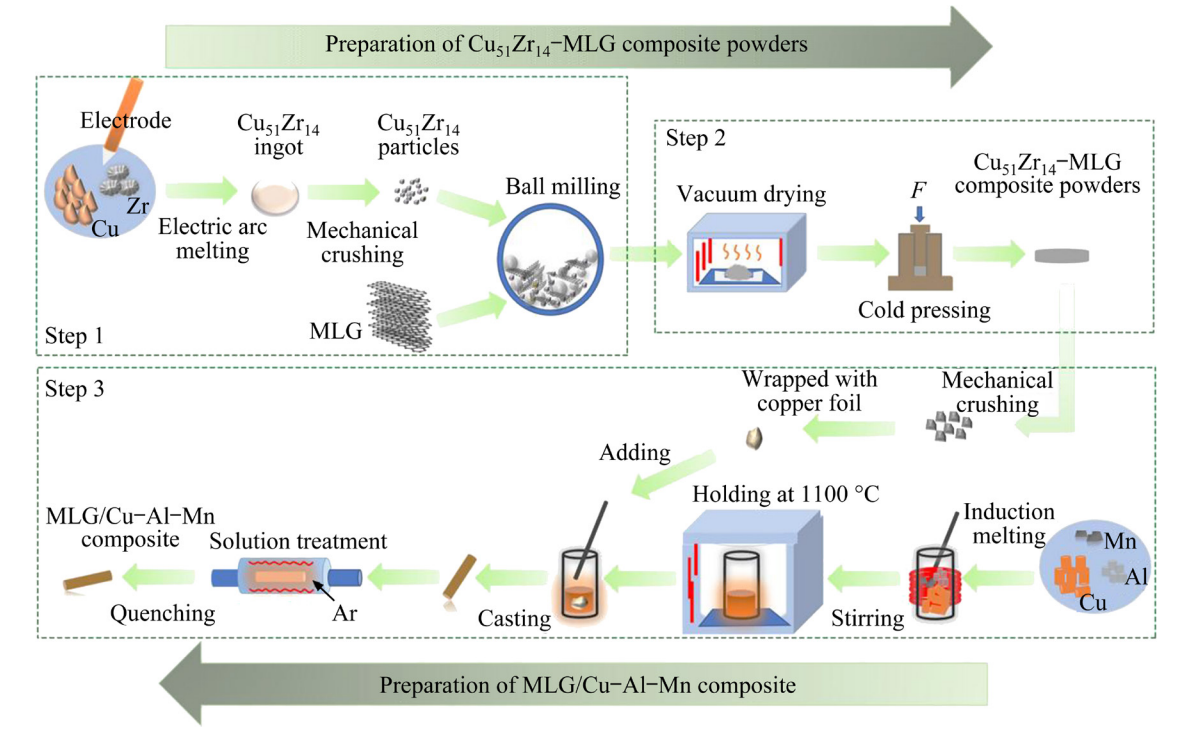


Fig. 2 Schematic illustration of preparation process of MLG/Cu-Al-Mn composites

10:1. Anhydrous alcohol was added as the wetmilling medium to prevent heating of the milling jar and excessive adhesion and aggregation of powders during ball milling.

(2) Step 2: Cold pressing of Cu₅₁Zr₁₄ and MLG composite powders

After ball milling, the resultant Cu₅₁Zr₁₄–MLG composite powders were placed into a vacuum drying oven and dried at 80 °C. Then, they were cold pressed into a disc with a diameter of 20 mm and a height of 2 mm on hydraulic equipment under a pressure of 200 MPa.

(3) Step 3: Preparation of MLG/Cu-Al-Mn composites

The Cu-11.9Al-2.5Mn (wt.%) SMA was melted in an induction furnace by using pure Cu, Al (purity ≥99.9 wt.%, Tianjin Nonferrous Metals Company, China) and pure Mn (purity ≥99.9 wt.%, Qinghe County Benyu Metal Materials Co., Ltd., China) as raw materials. When the temperature reached 1100 °C, the Cu₅₁Zr₁₄-MLG composite blocks with a diameter of about 3 mm (obtained by mechanically crushing the disc) wrapped with copper foil were added. In this step, the content of Cu₅₁Zr₁₄ inoculant was controlled to be 1.0 wt.%, and the content of MLG was controlled to be 0.1, 0.15, 0.2 and 0.25 wt.%, respectively. Then, the melt was poured into a steel die after stirring. After that, the as-cast MLG/Cu-Al-Mn composite was subjected to solution treatment at 900 °C for 600 s followed by water quench [28,29]. The uninoculated Cu-Al-Mn SMA and the Cu-Al-Mn SMA inoculated by 1.0 wt.% Cu₅₁Zr₁₄ inoculant were also prepared as contrastive specimens.

2.2 Characterization

BX41M Olympus optical microscope (OM) and Quanta 450 FEG SEM were used to observe the microstructures. Before observation, the specimens were ground, polished and etched by FeCl₃–HCl corrosion solution. SISC IAS V8.0 image software was used to estimate the average grain size via the linear intercept method [30]. Bruker D8 Discover XRD with Cu K_{α} radiation and Raman spectroscopy were used to characterize the phase component. JEOL 8530F electron probe microanalysis (EPMA) and Tecnai G2 F30 transmission electron microscopy (TEM) were used to investigate the morphology and distribution of MLG in the MLG/Cu–Al–Mn composites.

2.3 Performance tests

Damping property of the composites was measured by TA Q800 dynamic mechanical analyzer (DMA), and the used specimens have a dimension of 35 mm × 10 mm × 2 mm. Tensile properties were measured at room temperature by INSTRON universal testing machine (UTM) with a speed of 1 mm/min, and the specimens with a gauge length of 25 mm and a diameter of 5 mm were machined according to the GB/T228.1—2010 (ISO 6892-1: 2016) standard. The micro-hardness was tested on HMV-2T Vickers hardness tester with a load of 200 g and a loading time of 15 s.

3 Results and discussion

3.1 Characterization of specimens

Figures 3(a, b) show the XRD patterns of the MLG, Cu₅₁Zr₁₄ inoculant and Cu₅₁Zr₁₄-MLG composite powders ball-milled for 5 and 10 h. The diffraction peak at $2\theta=26^{\circ}$ is the characteristic peak of graphene, and the other peaks correspond to the Cu₅₁Zr₁₄ inoculant. No other peaks can be detected, indicating that there is no chemical reaction between MLG and inoculant. The volume fractions of Cu₅₁Zr₁₄ and MLG in the composite powders quantified from the XRD data are 59.7% and 40.3% (ball-milled for 5 h) as well as 60.5% and 39.5% (ball-milled for 10 h), and corresponding mass fractions are 85% and 15% as well as 85.5% and 14.5%, which are close to the set mass ratio of 5:1. It can also be found from Fig. 3(b) that the peak positions of Cu₅₁Zr₁₄ inoculant remain unchanged before and after ball-milling, but the peak widths are broadened, which should be caused by grain refinement. Figure 3(c) shows the Raman spectra of the MLG and ball-milled Cu₅₁Zr₁₄-MLG composite powders. It can be seen that the value of I_D/I_G only increases slightly with prolonging the ball-milling time, indicating that MLG in the composite powders is low-defect and still fairly ordered [31-34]. Moreover, the D, G and 2D peaks of the MLG in the Cu₅₁Zr₁₄-MLG composite powders shift to the high frequency compared with the original MLG, which can be ascribed to the internal stress remaining in the MLG after ball-milling [35].

Figures 4(a–c) and 4(d–g) show the SEM images of the $Cu_{51}Zr_{14}$ –MLG composite powders ball-milled for 5 and 10 h, respectively. From Figs. 4(a, b, d, e), it can be seen that the $Cu_{51}Zr_{14}$

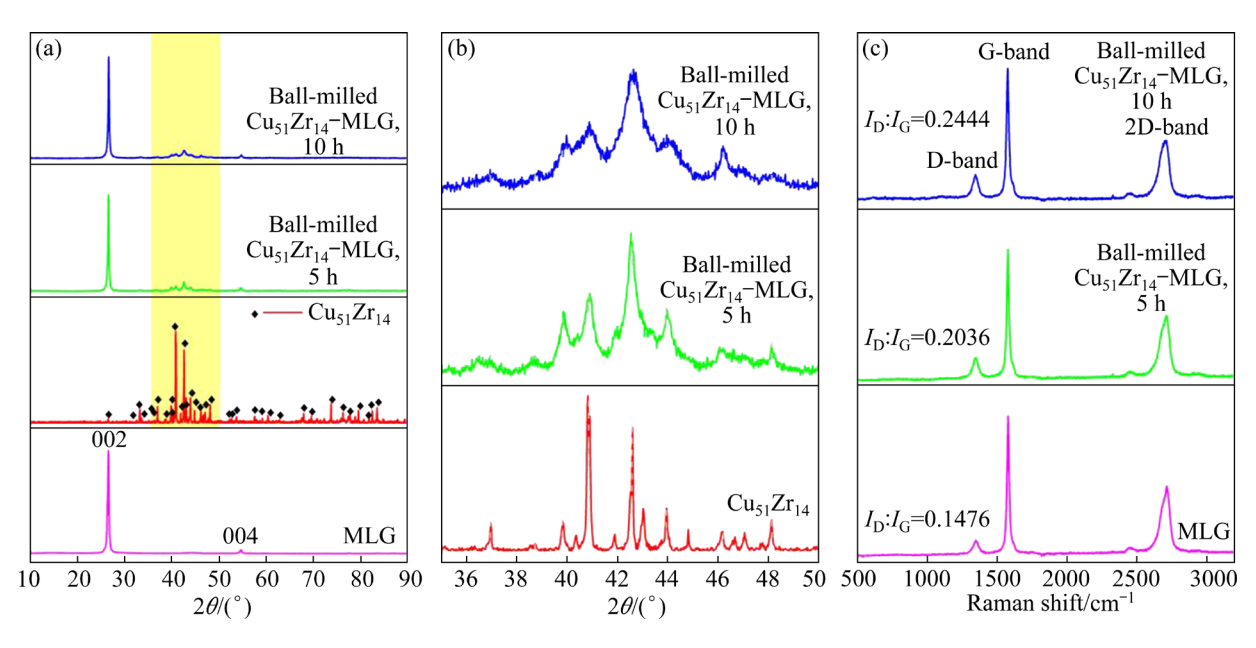


Fig. 3 XRD patterns of MLG, Cu₅₁Zr₁₄ inoculant and ball-milled Cu₅₁Zr₁₄–MLG (mass ratio of 5:1) composite powders (a); enlarged view (b) of yellow area in (a); Raman spectra of MLG and ball-milled Cu₅₁Zr₁₄–MLG composite powders (c)

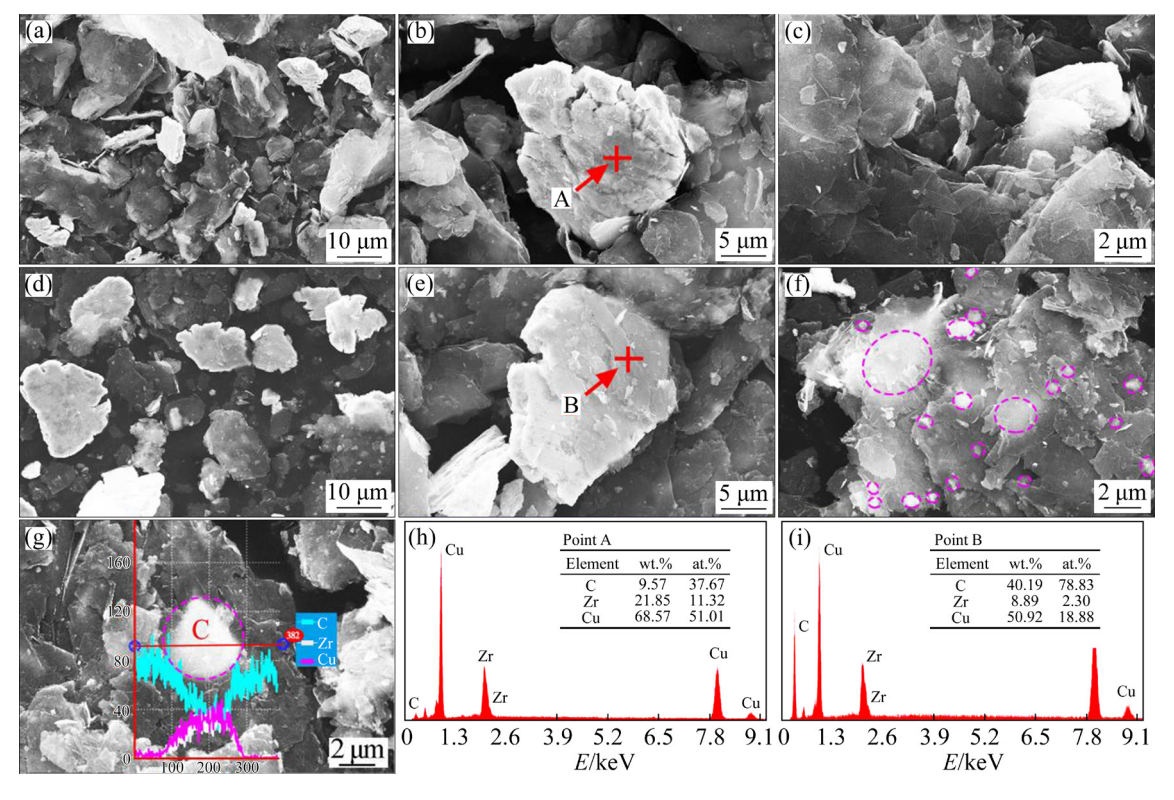


Fig. 4 SEM images of Cu₅₁Zr₁₄–MLG (mass ratio of 5:1) composite powders ball-milled for 5 h (a–c) and 10 h (d–g); EDS results of Points A (h) and B (i)

particles have been broken into fine particles (compared with the original Cu₅₁Zr₁₄ particles shown in Fig. 1(a)). Moreover, from the EDS results of Points A and B shown in Figs. 4(h, i), it

can be found that MLG fragments adhere to the surface of the $Cu_{51}Zr_{14}$ particles, and the amount of MLG fragments increases with the increase of ball milling time. From Figs. 4(f, g), it can also be

found that some very fine Cu₅₁Zr₁₄ particles are embedded in the lamellae of MLG, forming the special "MLG–Cu₅₁Zr₁₄–MLG" sandwich structure. Obviously, MLG and Cu₅₁Zr₁₄ particles in the composite powders ball milled for 10 h are more fully mixed, so 10 h is selected as the appropriate

ball milling time in this study.

Figures 5 and 6 show the optical micrographs, average grain size and XRD patterns of the MLG/Cu–Al–Mn composites and the contrastive specimens. There is no MLG in the specimens shown in Figs. 5(b, d). From Figs. 5(f, h), it can be

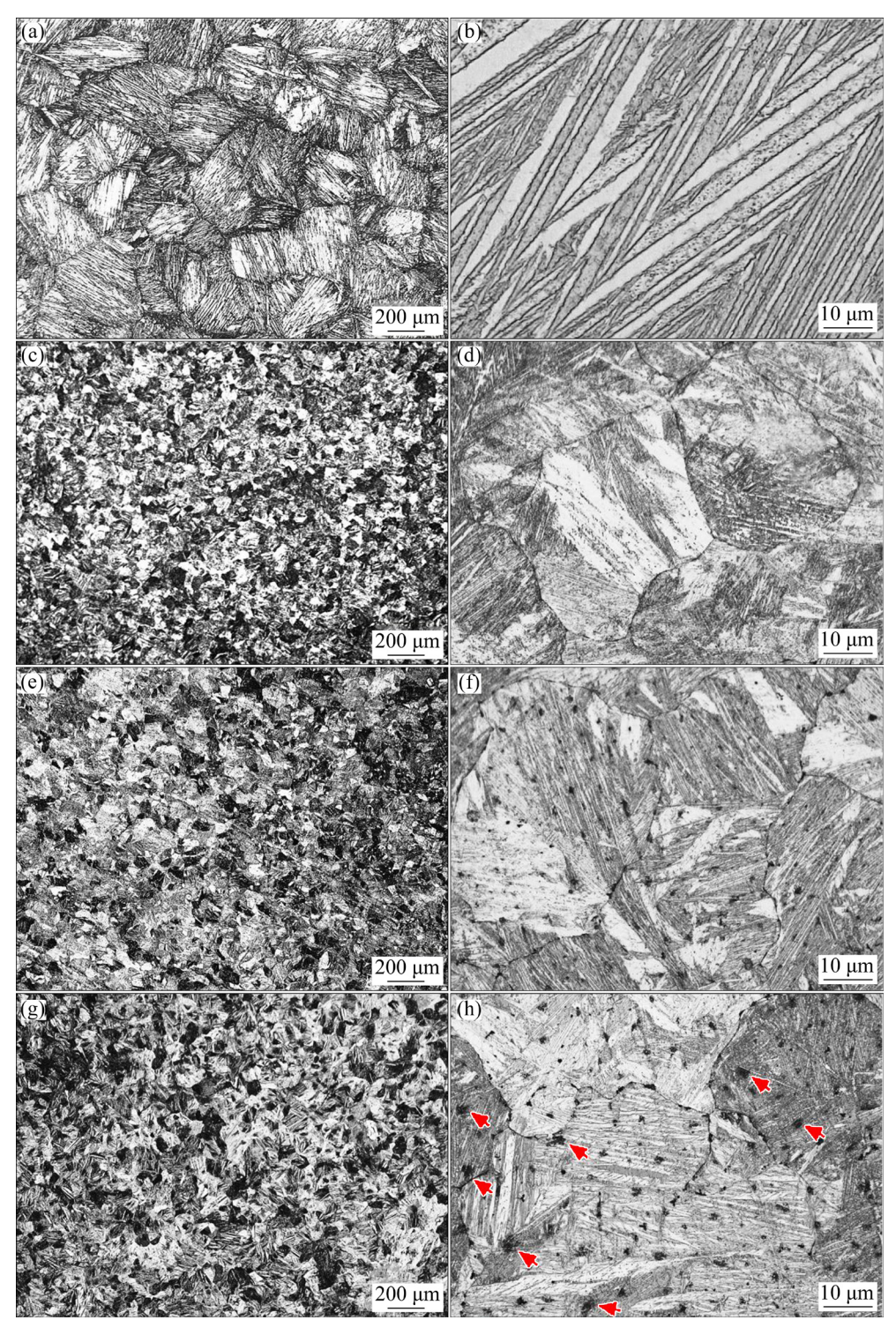


Fig. 5 Optical micrographs of specimens: (a, b) Original Cu–Al–Mn SMA (Sample 1); (c, d) With 1.0 wt.% $Cu_{51}Zr_{14}$ (Sample 2); (e, f) With 1.0 wt.% $Cu_{51}Zr_{14}$ and 0.2 wt.% MLG (Sample 5); (g, h) With 1.0 wt.% $Cu_{51}Zr_{14}$ and 0.25 wt.% MLG (Sample 6)

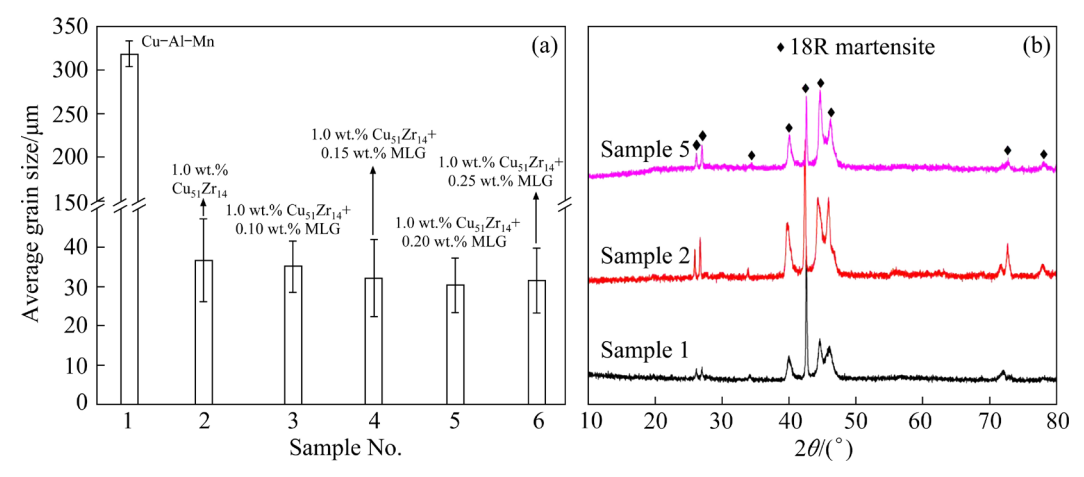


Fig. 6 Average grain size (a) and XRD patterns (b) of MLG/Cu-Al-Mn composites and contrastive specimens

seen that the MLG is dispersed within grains and at grain boundaries (GBs). Figure 6(a) shows that the grains are further refined after adding MLG compared with Cu-Al-Mn SMA inoculated only by Cu₅₁Zr₁₄, which can be ascribed to the pinning effect of dispersed MLG on GBs. Therefore, the growth of grains of the Cu-Al-Mn SMA is efficiently inhibited during heat treatment [26,36]. However, the grain size does not monotonously decrease with the increase of the content of MLG (for example, when the content of MLG reaches 0.25 wt.%, the grain size begins to increase), which can be attributed to the aggregation of excess MLG (as marked by arrows in Fig. 5(h)) [36,37]. It can be found from Fig. 6(b) that only the martensite phase can be detected after adding MLG, indicating that there is no chemical reaction between MLG and the Cu-Al-Mn matrix.

Figure 7 shows the EPMA maps of 0.20 wt.% MLG/Cu–Al–Mn composite. From Fig. 7(e), it can be found that the Cu₅₁Zr₁₄ particles are uniformly distributed in the Cu–Al–Mn matrix. From Fig. 7(f), a small amount of aggregated MLG and a large amount of MLG fragments can be clearly seen, and the Cu₅₁Zr₁₄ particles can also be found at some locations where MLG fragments are detected, as marked by the red dotted circles in Figs. 7(e, f).

In order to make clear the distributions of MLG and Cu₅₁Zr₁₄ particles in the composites and their relationship, detailed SEM observations and EDS analysis on the 0.20 wt.% MLG/Cu–Al–Mn composite were conducted, and the results are shown in Fig. 8. It can be seen from Figs. 8(a, b) that fine black floccules marked by green arrows are uniformly dispersed in the Cu–Al–Mn matrix.

According to the image with high magnification shown in Fig. 8(c') and the EDS results of Areas A and B shown in Figs. 8(f) and (g), respectively, it can be identified that the white flake in the middle of black floccule is MLG, and the black depression regions around it should be caused by the falling-off of MLG. As shown in Figs. 8(d, d'), white plum-shaped flakes marked by red arrows are embedded in the martensite laths, and according to the EDS result of Area C shown in Fig. 8(h), the white plum-shaped flakes contain a large amount of Zr element and a certain amount of C element. Combined with the analysis on Figs. 4(b, e, h, i), they should be Cu₅₁Zr₁₄ covered by MLG flakes. From Figs. 8(e, e'), the flocculent MLG can be found, and the EDS result of Area D shows that the white plum-shaped flake packaged by the flocculent MLG contains a certain amount of Zr element and a large amount of C element, while the EDS result of Area E shows that the flocculent MLG without white flake contains more C element but almost no Zr element, which is consistent with the results shown in Fig. 4(g). Therefore, the flocculent MLG shown in Figs. 8(e, e') has the same "MLG-Cu₅₁Zr₁₄-MLG" sandwich structure, as shown in Figs. 4(f, g).

Figure 9 shows the schematic diagram of the evolution process of the Cu₅₁Zr₁₄–MLG composite powders. As shown in Fig. 9(b), the ball-milled composite powders contain Cu₅₁Zr₁₄ flakes adhered with MLG fragments, small Cu₅₁Zr₁₄ particles and "MLG–Cu₅₁Zr₁₄–MLG" sandwich structure. As shown in Fig. 9(c), after the composite powders are put into the Cu–Al–Mn melt, although some MLG fragments may float up in the Cu–Al–Mn melt after

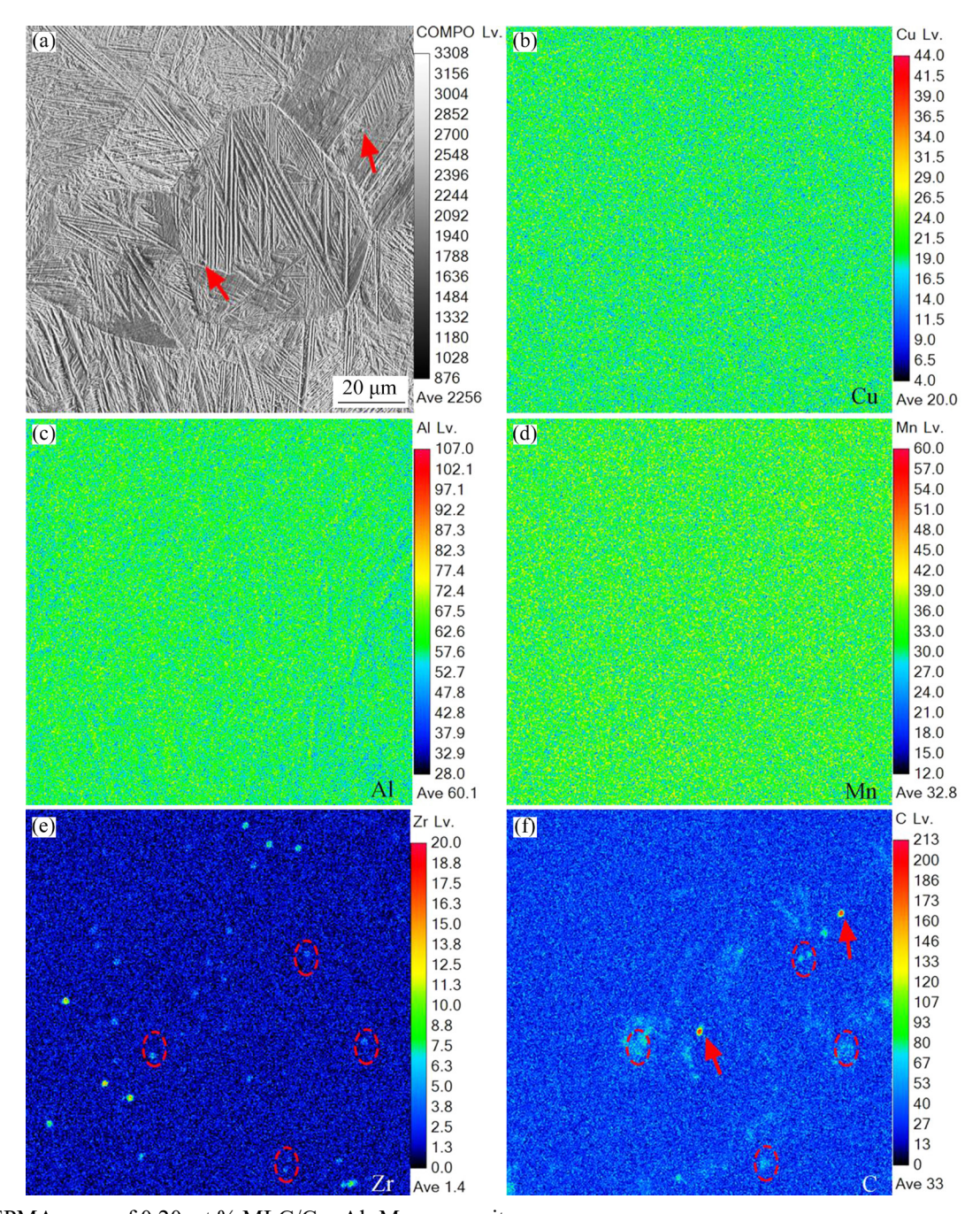


Fig. 7 EPMA maps of 0.20 wt.% MLG/Cu-Al-Mn composite

dropping-off of the Cu₅₁Zr₁₄ particles during the stirring, most of them can be dispersed in the Cu–Al–Mn melt due to the high viscosity of the Cu–Al–Mn melt at a casting temperature very close to the melting point of Cu–Al–Mn and the stable adhesion of MLG on the Cu₅₁Zr₁₄ particles, forming the structure shown in Fig. 8(c'). Meanwhile, the Cu₅₁Zr₁₄ inoculant is partially melted, forming the plum-shaped flakes (with small Cu₅₁Zr₁₄ particles acting as the nucleation centers of the Cu–Al–Mn melt). The size of the "MLG–Cu₅₁Zr₁₄–MLG" sandwich structure decreases, and with the stirring

in the inoculation process, the structure is gradually dispersed in the matrix of Cu–Al–Mn SMA. The uniform distribution of the above three structures containing MLG in the Cu–Al–Mn SMA (as shown in Fig. 9(d)) shows that the problem mentioned in the introduction section that MLG is difficult to disperse uniformly in the Cu–Al–Mn SMA can be skillfully solved by using the technique in this study.

TEM observations were conducted to further investigate the interfacial structure and microstructural characteristics of the MLG/Cu-Al-Mn

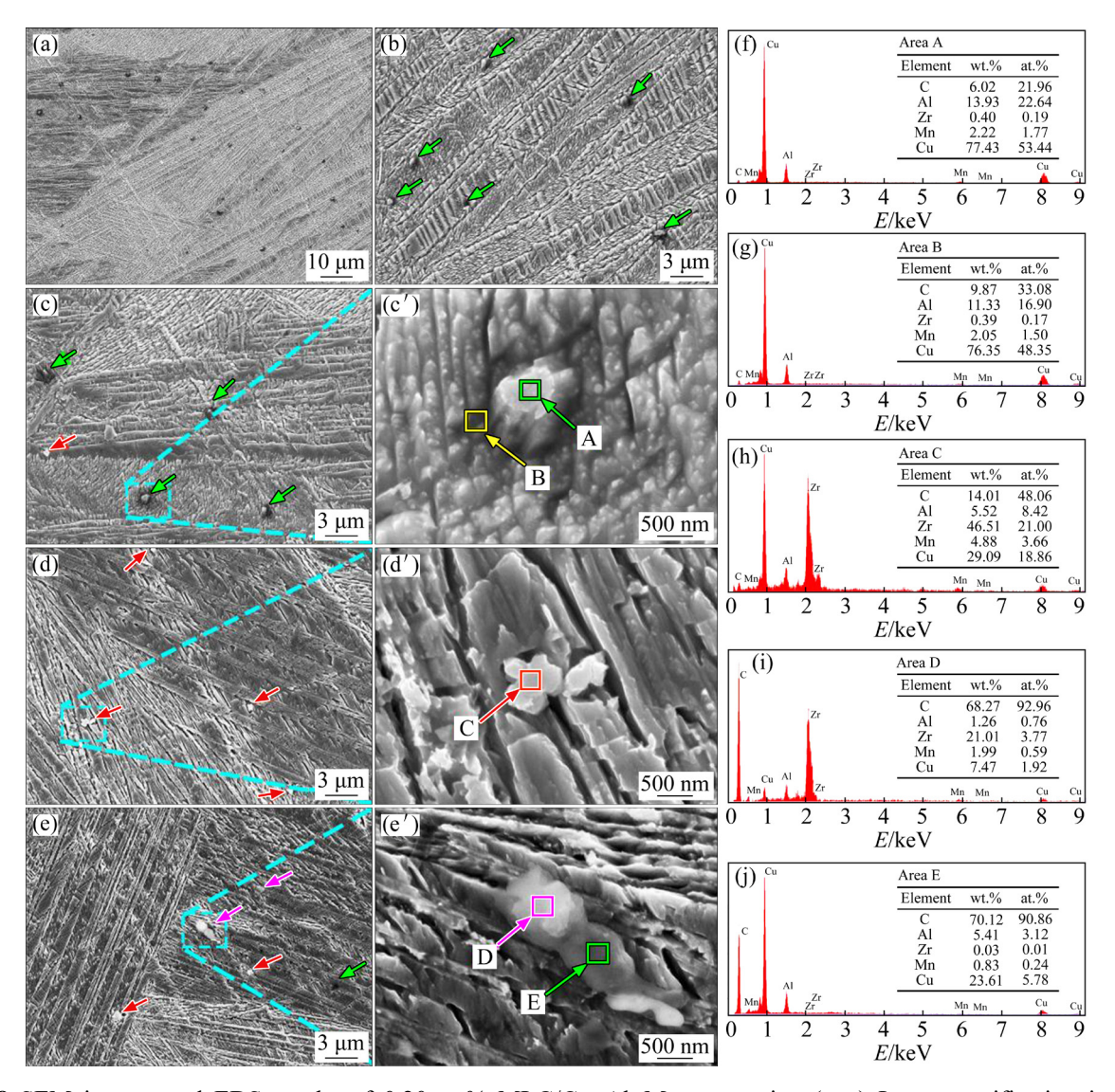


Fig. 8 SEM images and EDS results of 0.20 wt.% MLG/Cu-Al-Mn composite: (a-e) Low magnification images; (c'-e') High magnification images of marked areas; (f-j) EDS results of Areas A-E

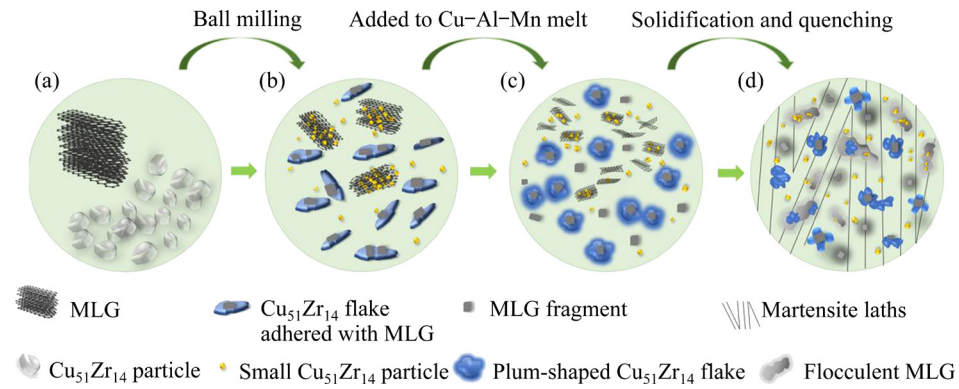


Fig. 9 Schematic illustration of evolution process of $Cu_{51}Zr_{14}$ –MLG composite powders: (a) Original MLG and $Cu_{51}Zr_{14}$ particles; (b–d) MLG and $Cu_{51}Zr_{14}$ composite powders after ball milling

composites. From Fig. 10, Cu₅₁Zr₁₄ particles, MLG fragments and Cu₅₁Zr₁₄ particles adhered with MLG can all be found. Figure 10(c) shows the high-

resolution TEM (HRTEM) image of the MLG/Cu-Al-Mn interface taken from Area B in Fig. 10(a). It can be seen that the interface of

MLG/Cu-Al-Mn is clear and straight, and there is no intermediate layer or interface inclusion. From Fig. 10(c), dislocations are found at the MLG/Cu-Al-Mn interface. The appearance of dislocations is due to the difference in the coefficient of thermal expansion (CTE) between MLG and Cu-Al-Mn matrix [38]. Such thermal mismatch dislocations can also be found in Fig. 10(i). They are located in the Cu-Al-Mn matrix around the MLG (marked by yellow and green arrows). The MLG has a hindering effect on the movement of dislocations. Under applied external stresses, the multiplication and entanglement of dislocations can occur in these regions, which contributes to the improvement of the mechanical properties of the composites.

3.2 Damping property

Figure 11 shows the damping behaviors of the MLG/Cu–Al–Mn composites and contrastive specimens. At around 400 °C, a damping peak appears. According to our previous work, this peak increases with increasing the heating rate \dot{T} or decreasing the measuring frequency f [39]. In addition, it is found that there is an endothermal peak at around 400 °C on the differential scanning calorimetry (DSC) curves of the Cu–Al–Mn SMA during the heating process [19], indicating that a first-order phase transition takes place at this temperature. Therefore, it can be confirmed that this peak originates from the reverse martensite transformation (MT) of the Cu–Al–Mn SMA. It is

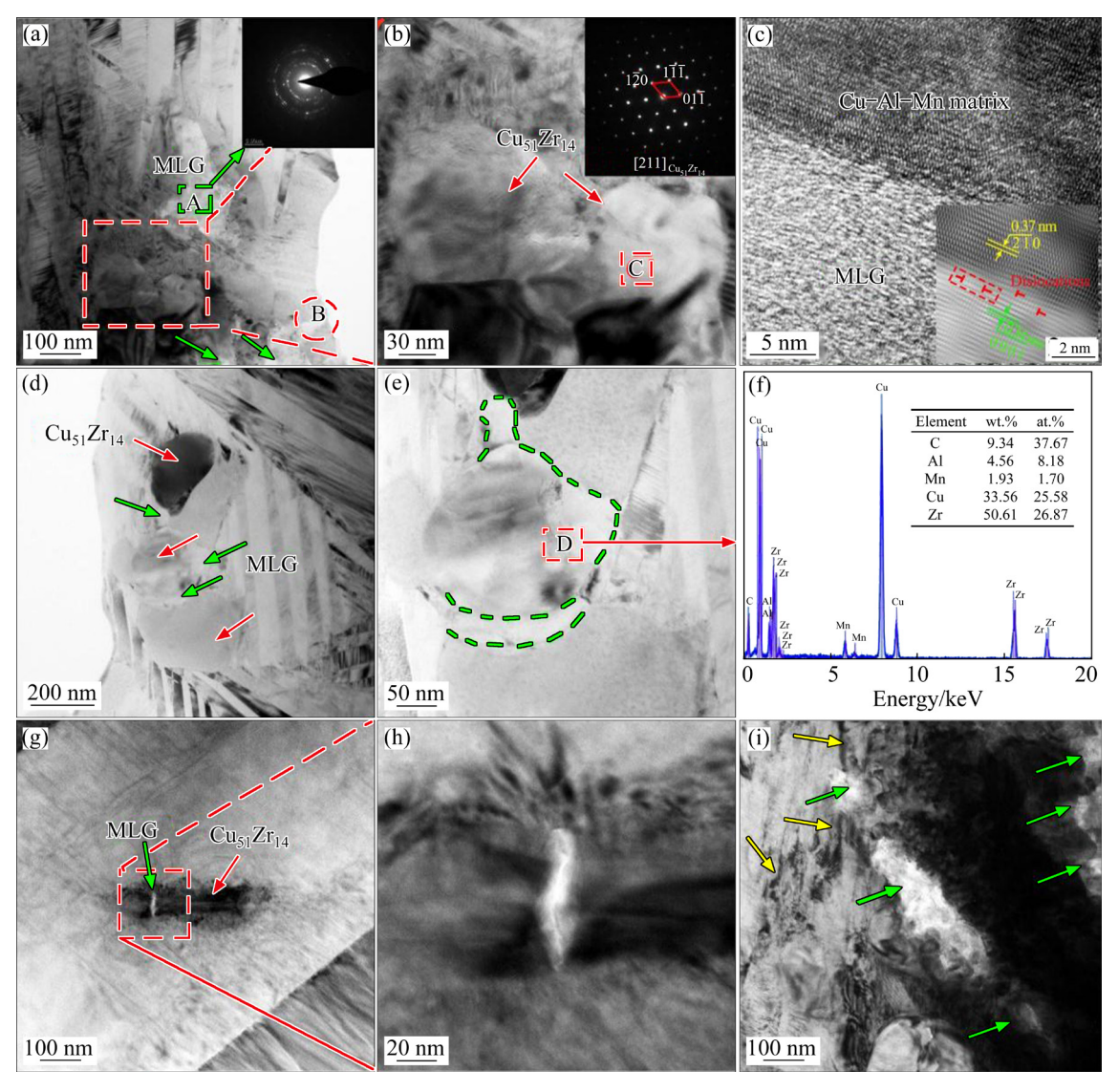


Fig. 10 TEM images of 0.20 wt.% MLG/Cu–Al–Mn composite: (a, b) MLG fragments, Cu₅₁Zr₁₄ particles and their selected-area electron diffraction (SAED) patterns; (c) HRTEM of MLG/Cu–Al–Mn interface taken from Area B in (a) and IFFT image; (d, e) Cu₅₁Zr₁₄ particles surrounded by MLG; (f) EDS result of Point D in (e); (g, h) Cu₅₁Zr₁₄ particle adhered with MLG; (i) Dislocations near MLG

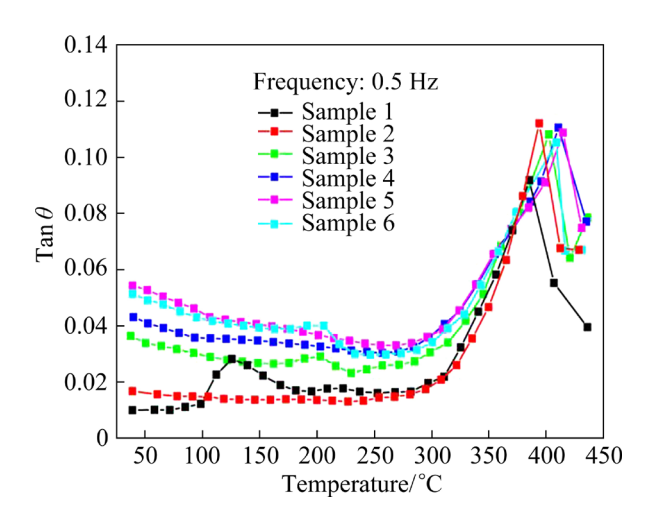


Fig. 11 Damping behaviors of MLG/Cu–Al–Mn composites and contrastive specimens

obvious that after adding MLG, the damping peak shows no significant change, but the room damping is significantly improved. With increasing the content of MLG, the damping increases first and then decreases. When the content of MLG is 0.20 wt.%, the highest damping can be obtained. The room-temperature damping reaches 0.0558, which is nearly 5 and 3 times that of the original and inoculated Cu-Al-Mn SMAs, respectively. This can be attributed to the high energy dissipation caused by the interfacial friction of MLG due to its lamellar structure and abundant interfaces [40]. The interlaminar interactions including van der Waals force, electrostatic attraction and interlayer radial loading, and the special surface characteristics of graphene such as defects, roughness, edge steps and wrinkled morphology (as shown in Figs. 1(b, c)) benefit the interfacial friction, and contribute a lot to the improvement of damping capacity [41-43]. LU et al [41] reported that the wrinkles with large coefficients of friction (COF) indeed play a dominant role in delaying slip occurrences. They believed that there are three types of interaction in the wrinkled interfaces as a result of the random orientation of the wrinkles. And all these interactions can cause severe distortion of the wrinkles due to the large friction forces involved and present high energy dissipation under the mutual slip of graphene layers. In addition, as shown in Figs. 8 and 10, there are a lot of MLG/Cu-Al-Mn and MLG/Cu₅₁Zr₁₄ interfaces in the composites. Under the applied cyclic stresses, these interfaces can also efficiently dissipate mechanical energy through the friction between them, which contributes to improving damping. Moreover, another significant contribution to damping is related to the generation of dislocations near MLG/Cu–Al–Mn interfaces and around MLG, as shown in Figs. 10(c, i). The mechanism of dislocation damping can be explained by the Granato–Lücke theory, which illustrates that dislocations are the primary sources for dissipation of elastic strain energy (i.e., damping) in crystalline metals and alloys [44,45].

The grain size also affects the damping. It can be seen from Fig. 6(a) that the addition of MLG leads to a further decrease in average grain size. This has been reported in our previous work that the finer the grains are, the higher the density of martensite interfaces is, and the higher damping capacity is for the Cu–Al–Mn SMA [19,46]. Therefore, adding MLG is conducive to improving the damping of the Cu–Al–Mn SMA. Nevertheless, the excessive addition of MLG is undesirable. From Fig. 11, it is apparent that the damping in the martensite state decreases slightly when the content of MLG increases to 0.25 wt.%. It is believed that the agglomeration of excessive MLG should be responsible for this [26].

3.3 Mechanical properties

Figure 12 shows the mechanical properties of the MLG/Cu–Al–Mn composites and contrastive specimens. It is seen that the tensile strength σ_b , elongation δ and hardness of the MLG/Cu–Al–Mn composites are higher than those of the original and inoculated Cu–Al–Mn SMAs. When the content of MLG reaches 0.20 wt.%, the highest σ_b of 801.5 MPa, δ of 10.8% and hardness of HV 308

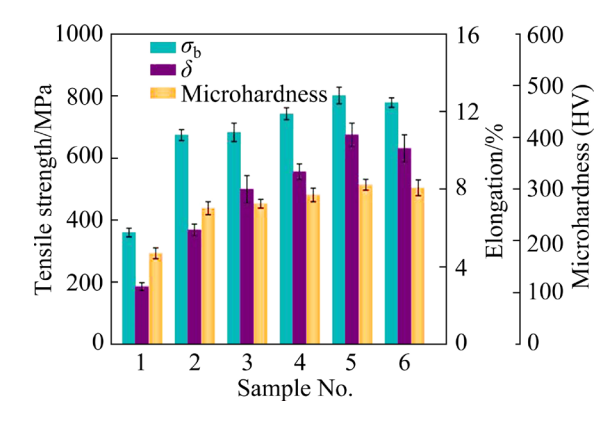


Fig. 12 Tensile strength, elongation and hardness of MLG/Cu–Al–Mn composites and contrastive specimens

can be obtained. They are 2.2, 3.6 and 1.8 times those of original Cu–Al–Mn SMA, respectively. However, three values decrease slightly with further increasing the content of MLG.

The strengthening effect of MLG on the composites is mainly due to the generation of thermal mismatch dislocations [47] and the effective load transfer [48,49]. Since MLG can only lead to slight grain refinement, the contribution of grain refinement is relatively low. The generation of thermal mismatch dislocation is due to the large mismatch of CTE between MLG and Cu-Al-Mn matrix. The CTE of MLG at room temperature is -6×10^{-6} °C⁻¹ [50], and that of the Cu–Al–Mn matrix is 5.79×10⁻⁵ °C⁻¹ [51]. The large difference in CTE can result in huge residual stress in the Cu-Al-Mn matrix adjacent to MLG [38]. When it is higher than the yield stress of the Cu-Al-Mn SMA, microplastic deformation occurs, leading to the generation of a large number of dislocations and resulting in the dislocation strengthening effect on the composites [50,52]. As for the load transfer mechanism, loads can be transferred from the metal matrix to MLG through interfacial shear stress. Thus, the volume fraction of MLG and the interfacial bonding effect between MLG and Cu-Al-Mn matrix are the crucial influencing factors [49,50,52]. As shown in Fig. 10(c), there is a good interfacial bonding between MLG and Cu-Al-Mn matrix, which improves the mechanical properties. Nevertheless, excessive addition of MLG is undesirable, because the locations

containing agglomerated MLG are equivalent to micropores and can lead to stress concentration and micro-cracks, which can decrease the mechanical properties [24,37].

Tensile fracture morphologies of the MLG/ Cu-Al-Mn composites and contrastive specimens are shown in Fig. 13. From Fig. 13(a), it is seen that the original Cu-Al-Mn SMA presents typical characteristics of intergranular brittle fracture. From Fig. 13(b), the fracture surface of the Cu-Al-Mn SMA inoculated by Cu₅₁Zr₁₄ inoculant begins to show relatively shallow dimples, indicating that the ductility of Cu-Al-Mn SMA is improved. Moreover, for the MLG/Cu-Al-Mn composites, denser and deeper dimples appear on their fracture surfaces. Meanwhile, second-phase particles are found inside these dimples. These particles generally serve as the nucleation centers of micropores. The micropore aggregation fracture is just the main mechanism of ductile fracture, so adding MLG efficiently improves the ductility. However, Fig. 13(f) shows that when excessive MLG is added, holes and gaps are formed in the composites (marked by red and green arrows, respectively). The spatial barrier of agglomerated MLG prevents the metal melt from flowing into the dendrite gap [49]. As a consequence, both the strength and ductility of the composites decrease.

In order to further show the effect of MLG on the fracture of MLG/Cu-Al-Mn composites, Fig. 14 show SEM images with high magnification and EDS results. From Figs. 14(a, a'), the second-

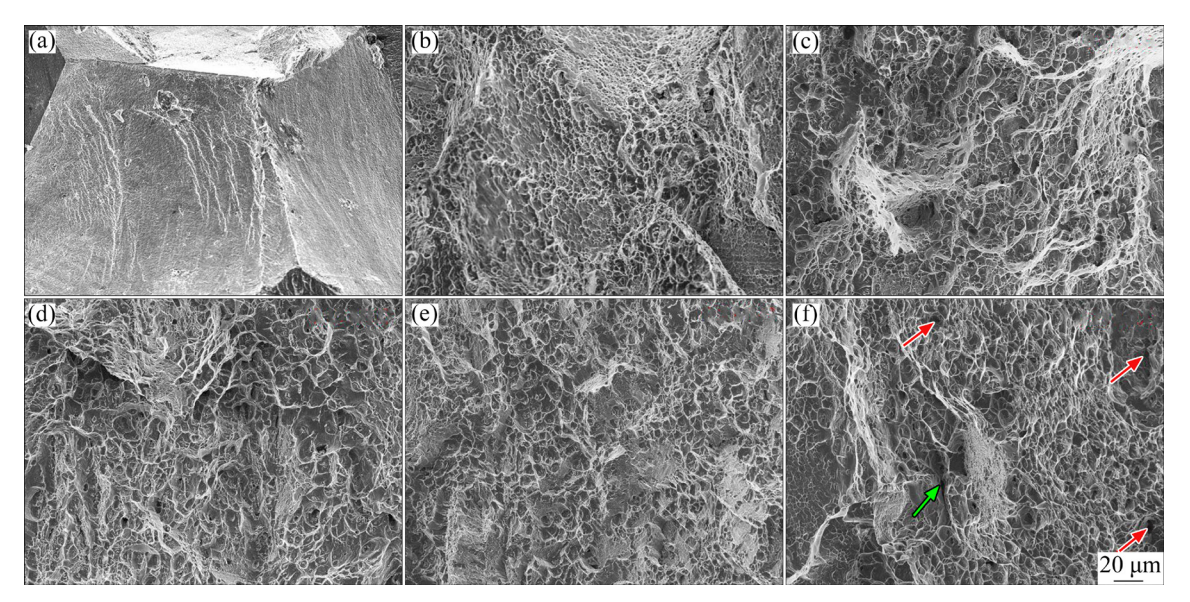


Fig. 13 Tensile fracture morphologies of samples: (a) Sample 1; (b) Sample 2; (c) Sample 3; (d) Sample 4; (e) Sample 5; (f) Sample 6

phase particles in dimples of the inoculated specimens are almost invisible, whereas from Figs. 14(b–e), particles (marked by red arrows) and pulled-out flakes (marked by green arrows) can be clearly seen in dimples. According to the EDS results of Points C, D and E in Figs. 14(d'), the particles are rich in Zr element, and the pulled-out flakes are rich in C element. Therefore, the particles and pulled-out flakes can be identified as Cu₅₁Zr₁₄ and MLG, respectively. The pull-out of the reinforcements in composites is usually considered one of the main factors of strengthening and

toughening [37,49]. During the pull-out process of MLG, the debonding of MLG/Cu–Al–Mn interface, the friction between MLG and Cu–Al–Mn matrix, and the bridging and final fracture of MLG consume a lot of energy, which can effectively improve the toughness of composites. In addition, MLG can also impede the propagation of cracks through the crack-tip-shielding mechanism [53]. From Fig. 14(e'), when excessive MLG is added, MLG agglomerates (marked by green arrows) in the composite, which is detrimental to the mechanical properties of the composites.

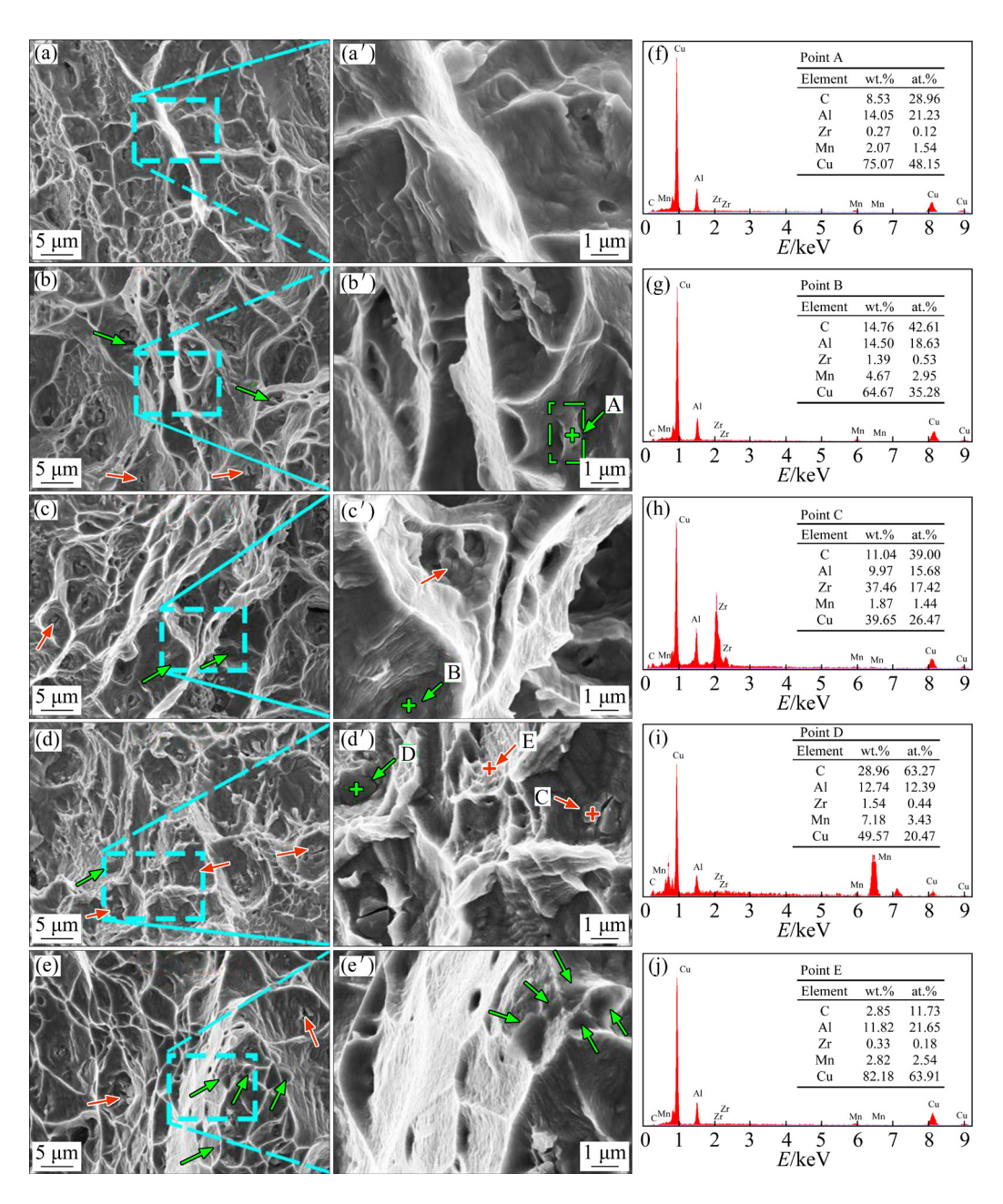


Fig. 14 Tensile fracture morphologies of Cu–Al–Mn SMA with 1.0 wt.% Cu₅₁Zr₁₄ inoculant (a, a') and 1.0 wt.% Cu₅₁Zr₁₄ and 0.10 wt.% (b, b'), 0.15 wt.% (c, c'), 0.20 wt.% (d, d') and 0.25 wt.% (e, e') MLG; EDS results of Points A–E (f, g)

4 Conclusions

- (1) MLG can be successfully added to the Cu–Al–Mn SMA by preparing the preform of the cold-pressed MLG–Cu₅₁Zr₁₄ composite powders. In the resultant MLG/Cu–Al–Mn composites, MLG in fragmented or flocculent form has a good bonding with the Cu–Al–Mn matrix. MLG distributed at GBs can effectively prevent the migration of GBs during heat treatments, thereby preventing the coarsening of grains of the Cu–Al–Mn SMA. Thermal mismatch dislocations are formed near the MLG/Cu–Al–Mn interfaces and in the regions adjacent to MLG.
- (2) The damping of the MLG/Cu–Al–Mn composites is significantly improved, which can be attributed to the following three types of newly formed damping sources: The first one is MLG with high intrinsic damping due to its abundant lamellae and wrinkled interfaces; The second one is the thermal mismatch dislocations near the MLG/Cu–Al–Mn interfaces, which can dissipate mechanical energy through sliding; The third one is MLG/Cu–Al–Mn and MLG/Cu₅₁Zr₁₄ interfaces in the composites, which can efficiently dissipate mechanical energy via the friction.
- (3) The tensile mechanical properties of the MLG/Cu-Al-Mn composites are significantly improved. The maximum strength, elongation and hardness can reach 801.5 MPa, 10.8% and HV 308, respectively. The tensile fracture mode changes from intergranular brittle fracture to ductile fracture characterized by dimples. The strengthening of the composites can be attributed to grain refinement, generation of thermal mismatch dislocations and effective load transfer. The toughening of the composites is mainly related to the pull-out of MLG. The debonding of MLG/Cu-Al-Mn interface, the friction between MLG and Cu-Al-Mn matrix, and the bridging and final fracture of MLG can consume a lot of energy, which can remarkably improve the toughness.

CRediT authorship contribution statement

Zhi-xian JIAO: Investigation, Data curation, Writing — Original draft; **Qing-zhou WANG:** Conceptualization, Methodology, Project administration, Funding acquisition; **Yan-jun DING:** Validation,

Writing – Review & editing; Fu-xing YIN: Supervision, Funding acquisition; Chao-hui XU: Investigation; Cui-hong HAN: Investigation, Funding acquisition; Qi-xiang FAN: Investigation.

Declaration of competing interest

The authors declare that they have no known competing financial interests or personal relationships that could have appeared to influence the work reported in this paper.

Acknowledgments

This work was supported by the Natural Science Foundation of Hebei Province, China (No. E2021202017), the National Natural Science Foundation of China (No. 52061038), the Foundation Strengthening Program, China (No. 2019-JCJQ-ZD- 142-00), the Hebei Province Graduate Innovation Funding Project, China (No. CXZZBS2022032), the Jiangsu Provincial Policy Guidance Program (Special Project for the Introduction of Foreign Talents) Talent Introduction Program, China (No. BX2021024), and the Science Plan Foundation of Tianjin Municipal Education Commission, China (No. 2021KJ026).

References

- [1] GUO Li-peng, ZHANG Jin-ping, CHEN Xiao-qiang, ZHENG Shi-wei, YANG Shui-yuan, WANG Shu-liang, RUAN Jing-jing, WANG Cui-ping. Full shape memory effect of Cu-13.5Al-4Ni-6Fe shape memory martensite single crystal [J]. Transactions of Nonferrous Metals Society of China, 2023, 33: 1452-1459.
- [2] YIN Mo-yang, LI Zhou, XIAO Zhu, PANG Yong, LI Ya-ping, SHEN Zi-yan. Corrosion behavior of Cu-Al-Mn-Zn-Zr shape memory alloy in NaCl solution [J]. Transactions of Nonferrous Metals Society of China, 2021, 31: 1012-1022.
- [3] MOGHADDAM A O, KETABCHI M, BAHRAMI R. Kinetic grain growth, shape memory and corrosion behavior of two Cu-based shape memory alloys after thermomechanical treatment [J]. Transactions of Nonferrous Metals Society of China, 2013, 23: 2896–2904.
- [4] VRSALOVIĆ L, IVANIĆ I, KOŽUH S, GUDIĆ S, KOSE B, GOJIĆ M. Effect of heat treatment on corrosion properties of CuAlNi shape memory alloy [J]. Transactions of Nonferrous Metals Society of China, 2018, 28: 1149–1156.
- [5] GOMIDŽELOVIĆ L, POŽEGA E, KOSTOV A, VUKOVIĆ N, KRSTIĆ V, ŽIVKOVIĆ D, BALANOVIĆ L. Thermodynamics and characterization of shape memory Cu–Al–Zn alloys [J]. Transactions of Nonferrous Metals Society of China, 2015, 25: 2630–2636.
- [6] YANG Qing-wei, WANG Shan-ling, CHEN Jie, PENG

- Hua-bei, WEN Yu-huang. Strong heating rate-dependent deterioration of shape memory effect in up/step quenched Cu-based alloys: A ductile Cu-Al-Mn alloy as an example [J]. Acta Materialia, 2016, 111: 348–356.
- [7] CHANG S H, LIAO B S, GHOLAMI-KERMANSHAI M. Effect of Co additions on the damping properties of Cu–Al–Ni shape memory alloys [J]. Journal of Alloys and Compounds, 2020, 847: 156560.
- [8] SAUD S N, HAMZAH E, ABUBAKAR T, BAKHSHESHI-RAD H R. Correlation of microstructural and corrosion characteristics of quaternary shape memory alloys Cu–Al–Ni–X (X=Mn or Ti) [J]. Transactions of Nonferrous Metals Society of China, 2015, 25: 1158–1170.
- [9] GUNIPUTI B N, MURIGENDRAPPA S M. Influence of Gd on the microstructure, mechanical and shape memory, properties of Cu-Al-Be polycrystalline shape memory alloy [J]. Materials Science and Engineering A, 2018, 737: 245-252.
- [10] GERA D, SANTOS J, KIMINAMI C S, GARGARELLA P. Comparison of Cu–Al–Ni–Mn–Zr shape memory alloy prepared by selective laser melting and conventional powder metallurgy [J]. Transactions of Nonferrous Metals Society of China, 2020, 30: 3322–3332.
- [11] YANG Shui-yuan, ZHANG Fan, WU Jia-lin, LU Yong, SHI Zhan, WANG Cui-ping, LIU Xing-jun. Superelasticity and shape memory effect in Cu-Al-Mn-V shape memory alloys [J]. Materials & Design, 2017, 115: 17-25.
- [12] PANDEY A, HUSSAIN S, NAIR P, DASGUPTA R. Influence of niobium and silver on mechanical properties and shape memory behavior of Cu-12Al-4Mn alloys [J]. Journal of Alloys and Compounds, 2020, 836: 155266.
- [13] IACOVIELLOA F, COCCO V D, NATALI S, BROTZU A.
 Grain size and loading conditions influence on fatigue crack propagation in a Cu–Zn–Al shape memory alloy [J].
 International Journal of Fatigue, 2018, 115: 27–34.
- [14] ZHANG Xin, CUI Tian-yu, LIU Qing-suo, DONG Zhi-zhong, MAN Cheng. Effect of Nd addition on the microstructure, mechanical properties, shape memory effect and corrosion behavior of Cu–Al–Ni high-temperature shape memory alloys [J]. Journal of Alloys and Compounds, 2021, 858: 157685.
- [15] ZHANG M X, KELLY P M. Edge-to-edge matching and its applications. Part I: Application to the simple HCP/BCC system [J]. Acta Materialia, 2005, 53: 1073–1084.
- [16] BOLZONI L, BABU N H. On the grain refining efficacy of Ti-free hypoeutectic AlSi via AlTiB, AlB and AlNbB chemical inoculation [J]. Journal of Alloys and Compounds, 2020, 817: 152807.
- [17] LIU Shui-qing, WANG Xin, CUI Chun-xiang, ZHAO Li-chen, LI Nuo, ZHANG Zhe, DING Jin-hua, SHA Deng-hao. Enhanced grain refinement of in situ CeB6/Al composite inoculant on pure aluminum by microstructure control [J]. Journal of Alloys and Compounds, 2017, 701: 926–934.
- [18] YANG Jian, WANG Qing-zhou, YIN Fu-xing, CUI Chun-xiang. Effects of grain refinement on the structure and

- properties of a CuAlMn shape memory alloy [J]. Materials Science and Engineering A, 2016, 664: 215–220.
- [19] JIAO Zhi-xian, WANG Qing-zhou, YIN Fu-xing, CUI Chun-xiang, ZHANG Jian-jun, YAO Chang. Effects of Cu₅₁Zr₁₄ inoculant and caliber rolling on microstructures and comprehensive properties of a Cu-Al-Mn shape memory alloy [J]. Materials Science and Engineering A, 2020, 772: 138773.
- [20] KIM W J, LEE T J, HAN S H. Multi-layer graphene/copper composites: Preparation using high-ratio differential speed rolling, microstructure and mechanical properties [J]. Carbon, 2014, 69: 55–56.
- [21] DIXIT S, MAHATA A, MAHAPATRA D R, KAILAS S V, CHATTOPADHYAY K. Multi-layer graphene reinforced aluminum—Manufacturing of high strength composite by friction stir alloying [J]. Composites Part B-Engineering, 2018, 136: 63-71.
- [22] MU Xiao-nan, CAI Hong-nian, ZHANG Hong-mei, FAN Qun-bo, ZHANG Zhao-hui, WU Yan, Ge Yu-xin, WANG Duo-duo. Interface evolution and superior tensile properties of multi-layer graphene reinforced pure Ti matrix composite [J]. Materials & Design, 2018, 140: 431–441.
- [23] WANG Xue, XIAO Wei, WANG Li-gen, SHI Jing-min, SUN Lu, CUI Jian-dong, WANG Jian-wei. Investigation on mechanical behavior of multilayer graphene reinforced aluminum composites [J]. Physica E-Low-Dimensiona Systems & Nanos Trucyures, 2020, 123: 114172.
- [24] MU Xiao-nan, CAI Hong-nian, ZHANG Hong-mei, FAN Qun-bo, WANG Fu-chi, ZHANG Zhao-hui, WU Yan, GE Yu-xin, SHI Rui-zhou, WANG Duo-duo. Uniform dispersion of multi-layer graphene reinforced pure titanium matrix composites via flake powder metallurgy [J]. Materials Science and Engineering A, 2018, 725: 541–548.
- [25] KIM Y, LEE J, YEOM M S, SHIN J W, KIM H, CUI Y, KYSAR J W, HONE J, JUNG Y, JEON S, HAN S M. Strengthening effect of single-atomic-layer graphene in metal-graphene nanolayered composites [J]. Nature Communications, 2013, 4: 1–7.
- [26] CHU Ke, JIA Cheng-chang. Enhanced strength in bulk graphene-copper composites [J]. Physica Status Solidi A, 2014, 211: 184–190.
- [27] DUAN Duan-zhi, MA Yu-shan, DING Jian-jun, CHANG Zhan-dong, LIU Hai-bo, JIANG Zhuang-de. Effect of multilayer graphene addition on performance of brazed diamond drill bits with Ni-Cr alloy and its mechanism [J]. Ceramics International, 2020, 46: 16684–16692.
- [28] WANG Qing-zhou, LU Dong-Mei, CUI Chun-xiang, LIU Wei-jun, XU Men, YANG Jian. Effects of aging on the structure and damping behaviors of a novel porous Cu–Al–Mn shape memory alloy fabricated by sintering-dissolution method [J]. Materials Science and Engineering A, 2014, 615: 278–282.
- [29] XIAO Zhu, FANG Mei, LI Zhou, XIAO Tao, LEI Qian. Structure and properties of ductile Cu-Al-Mn shape memory alloy synthesized by mechanical alloying and powder metallurgy [J]. Materials & Design, 2014, 58:

451-456.

- [30] OLIVEIRA J P, ZENG Z, ANDREI C, BRAZ FERNANDES F M, MIRANDA R M, RAMIREZ A J, OMORI T, ZHOU N. Dissimilar laser welding of superelastic NiTi and Cu–Al–Mn shape memory alloys [J]. Materials & Design, 2017, 128: 166–175.
- [31] SAMANTARAY S S, ANEES P, PARAMBATH V B, RAMAPRABHU S. Graphene supported MgNi alloy nanocomposite as a room temperature hydrogen storage material–Experiments and theoretical insights [J]. Acta Materialia, 2021, 215: 117040.
- [32] FERRARI A C, MEYER J C, SCARDACI V, CASIRAGHI C, LAZZERI M, MAURI F, PISCANEC S, JIANG D, NOVOSELOV K S, ROTH S, GEIM A K. Raman spectrum of graphene and graphene layers [J]. Physical Review Letters, 2006, 97: 187401.
- [33] HE Chun-nian, ZHAO Nai-qin, SHI Chun-sheng, DU Xi-wen, LI Jia-jun. An approach to obtaining homogeneously dispersed carbon nanotubes in Al powders for preparing reinforced Al-matrix composites [J]. Advanced Materials, 2007, 19: 1128–1132.
- [34] AN Yu-min, HAN Jie-cai, ZHANG Xing-hong, HAN Wen-bo, CHENG Ye-hong, HU Ping, ZHAO Guang-dong. Bioinspired high toughness graphene/ZrB₂ hybrid composites with hierarchical architectures spanning several length scales [J]. Carbon, 2016, 107: 209–216.
- [35] SUN Jia-lin, ZHAO Jun, GONG Feng, LI Zuo-li, NI Xiu-ying. Design, fabrication and characterization of multi-layer graphene reinforced nanostructured functionally graded cemented carbides [J]. Journal of Alloys and Compounds, 2018, 750: 972–979.
- [36] ZHANG Dan-dan, ZHAN Zai-ji. Preparation of graphene nanoplatelets-copper composites by a modified semi-powder method and their mechanical properties [J]. Journal of Alloys and Compounds, 2016, 658: 663–671.
- [37] KHAN M, DIN R U, WADOOD A, SYED W H, AKHTAR S, AUNE R E. Effect of graphene nanoplatelets on the physical and mechanical properties of Al6061 in fabricated and T6 thermal conditions [J]. Journal of Alloys and Compounds, 2019, 790: 1076–1091.
- [38] GUAN Ren-guo, WANG Yu, SU Nan-yao, JI Zhi-gang, CHEN Biao. Fabrication of aluminum matrix composites reinforced with Ni-coated graphene nanosheets [J]. Materials Science and Engineering A, 2019, 754: 437–446.
- [39] WANG Qing-zhou, HAN Fu-shen, WANG Qiang. Low-frequency damping behavior of CuAlMn shape memory alloy [J]. Physica Status Solidi A, 2004, 201: 2910–2914.
- [40] LIN Guang-yuan, PENG Yi-fei, LI Yu-sen, LIANG Han-zheng, DONG Zhi-lei, ZHOU Yi-hu, YUE Zhen-ming, ZHANG Jie, XIONG Ding-Bang, ZHANG Di. Remarkable anisotropic wear resistance with 100-fold discrepancy in a copper matrix laminated composite with only 0.2 vol.% graphene [J]. Acta Materialia, 2021, 215: 117092.
- [41] LU Wen-jiang, QIN Fa-xiang, WANG Yun-fei, LUO Yang,

- WANG Huan, SCARPA F, LI Ji-xue, SESANA R, CURAL F, PENG Hua-xin. Engineering graphene wrinkles for large enhancement of interlaminar friction enabled damping capability [J]. ACS Applied Materials & Interfaces, 2019, 11: 30278–30289.
- [42] GAJUREL P, KIM M, WANG Q, DAI W T, LIU H T, CEN C. Vacancy-controlled contact friction in graphene [J]. Advanced Functional Materials, 2017, 27: 1702832.
- [43] ZANDIATASHBAR A, LEE G H, AN S J, LEE S, MATHEW N, TERRONES M, HAYASHI T, PICU C R, HONE J, KORATKAR N. Effect of defects on the intrinsic strength and stiffness of graphene [J]. Nature Communications, 2014, 5: 3186.
- [44] GRANATO A, LÜCKE K. Application of dislocation theory to internal friction phenomena at high frequencies [J]. Journal of Applied Physics, 1956, 27: 789–805.
- [45] LU An-liang, ZHAO Lei, LIU Yu, LI Zhi-qiang, XIONG Ding-bang, ZOU Jin, GUO Qiang. Enhanced damping capacity in graphene—Al nanolaminated composite pillars under compression cyclic loading [J]. Metallurgical and Materials Transactions A, 2020, 51: 1463–1468.
- [46] LIU Xiao-jin, WANG Qing-zhou, KONDRATÉV S Y, JI Pu-guang, YIN Fu-xing, CUI Chun-xiang, HAO Gang-ling. Microstructural, mechanical, and damping properties of a Cu-based shape memory alloy refined by an in situ LaB₆/Al inoculant [J]. Metallurgical and Materials Transactions A, 2019, 50: 2310–2321.
- [47] ZHANG Dan-dan, ZHAN Zai-ji. Strengthening effect of graphene derivatives in copper matrix composites [J]. Journal of Alloys and Compounds, 2016, 654: 226–233.
- [48] SUN Jia-lin, ZHAO Jun. Multi-layer graphene reinforced nano-laminated WC-Co composites [J]. Materials Science and Engineering A, 2018, 723: 1–7.
- [49] YANG Ming, WENG Lin, ZHU Han-xing, ZHANG Fan, FAN Tong-xiang, ZHANG Di. Leaf-like carbon nanotubegraphene nanoribbon hybrid reinforcements for enhanced load transfer in copper matrix composites [J]. Scripta Materialia, 2017, 138: 17–21.
- [50] LI Jian-chao, ZHANG Xue-xi, GENG Lin. Effect of heat treatment on interfacial bonding and strengthening efficiency of graphene in GNP/Al composites [J]. Composites Part A-Applied Science and Manufacturing, 2019, 121: 487-498.
- [51] ALÉS A, LANZINI F. Mechanical and thermodynamical properties of β-Cu−Al−Mn alloys along the Cu₃Al→ Cu₂AlMn compositional line [J]. Solid State Communications, 2020, 319: 113980.
- [52] RASHAD M, PAN F S, TANG A, ASIF M, AAMIR M. Synergetic effect of graphene nanoplatelets (GNPs) and multi-walled carbon nanotube (MW-CNTs) on mechanical properties of pure magnesium [J]. Journal of Alloys and Compounds, 2014, 603: 111–118.
- [53] XU Zeng-shi, SHI Xiao-liang, ZHAI Wen-zheng. Preparation and tribological properties of TiAl matrix composites reinforced by multilayer graphene [J]. Carbon, 2014, 67: 168–177.

通过添加 Cu₅₁Zr₁₄ 孕育剂颗粒承载的多层石墨烯提高 Cu-11.9Al-2.5Mn 形状记忆合金的综合性能

焦志娴1,2, 王清周2, 丁燕军3, 殷福星4, 徐超辉1, 韩翠红1, 范其香1

- 1. 天津职业技术师范大学 机械工程学院, 天津 300222;
- 2. 河北工业大学 材料科学与工程学院, 天津市材料层状复合与界面控制技术重点实验室, 天津 300130;
 - 3. 中南大学 材料科学与工程学院,长沙 410083;
 - 4. 广东省科学院 新材料研究所,广州 510651

摘 要:为了提高 Cu-11.9Al-2.5Mn 形状记忆合金(SMA)的综合性能,通过制备多层石墨烯(MLG)-CusiZr₁₄复合粉末冷压预制体,将 MLG 由 CusiZr₁₄孕育剂颗粒承载后添加并分散于该合金中。在所制备的新型 MLG/Cu-Al-Mn 复合材料中,碎片状或絮状的 MLG 与 Cu-Al-Mn 基体结合良好。 MLG 可以阻碍 Cu-Al-Mn SMA 晶粒的粗化,并在 MLG/Cu-Al-Mn 界面附近产生热失配位错。 MLG/Cu-Al-Mn 复合材料的阻尼和力学性能显著提高,当 MLG 的含量达到 0.2%(质量分数)时,其最高室温阻尼为 0.0558,抗拉强度为 801.5 MPa,伸长率为 10.8%,硬度为 HV 308。基于深入的显微组织观察,结合内耗理论以及金属的强韧化理论,对相关机理进行讨论。

关键词: Cu-Al-Mn 形状记忆合金; 多层石墨烯(MLG); 显微组织; 界面; 阻尼; 力学性能

(Edited by Bing YANG)